Efficient Methods for Solving Multi-Rate Partial Differential Equations in Radio Frequency Applications

JORGE OLIVEIRA
Department of Electrical Engineering
Technology and Management School - Polytechnic Institute of Leiria
Morro do Lena, Alto Vieiro, Apartado 4163, 2411-901 Leiria
PORTUGAL
oliveira@estg.ipleiria.pt

Abstract: - In telecommunication electronics, radio frequency applications are usually characterized by widely separated time scales. This multi-rate behavior arises in many kinds of circuits and increases considerably the computation costs of numerical simulations. In this paper we are mainly interested in electronic circuits driven by envelope modulated signals and we will show that the application of numerical methods based on a multi-rate partial differential equation analysis will lead to an efficient strategy for simulating this type of problems.

Key-Words: - Electronic circuit simulation, envelope-modulated signals, multi-rate partial differential equations.

1 Introduction

Dynamical behavior of electronic circuits can in general be described by ordinary differential equations (ODEs) in time, involving electric voltages, currents and charges and magnetic fluxes. For a general nonlinear circuit, Kirchhoff's laws lead to the system

$$p(y(t)) + \frac{dq(y(t))}{dt} = x(t), \qquad (1)$$

where $x(t) \in \mathbb{R}^n$ and $y(t) \in \mathbb{R}^n$ stand for the excitation and state-variable vectors, respectively. $p(y(t))$ represents memoryless linear or nonlinear elements, while $q(y(t))$ models dynamical linear or nonlinear elements (capacitors or inductors).

When the excitation $x(t)$ is a multi-rate stimulus the simulation process of such circuits is often a very challenging issue, especially if they are highly nonlinear. In the particular case in which we are interested (envelope modulated excited circuits) it happens that while envelopes are slowly varying signals, carriers are usually very high frequency sinusoids. Thus, obtaining the numerical solution of (1) is difficult because once we have signals with widely separated rates of variation we are forced to make discretizations on long time grids with extremely small time steps.

2 Multidimensional Problem

In this section we will begin by presenting a recent generic formulation for solving electronic circuits with widely separated time scales. As we will see, the key idea behind this strategy is to use multiple time variables, which enable multi-rate signals to be represented more efficiently. In our case, we will need two time variables and we will adopt the following procedure: for the slowly-varying parts (envelope) of the expressions of $x(t)$ and $y(t)$, t is replaced by t_1; for the fast-varying parts (carrier) t is replaced by t_2. This will result in bivariate representations for the excitation and the solution, and we will denote these two argument functions by $\hat{x}(t_1, t_2)$ and $\hat{y}(t_1, t_2)$.

2.1 Bivariate Representation

Simulating circuits using numerical schemes require time steps spaced closely enough to represent signals accurately. For concreteness let us consider the slowly-varying envelope signal $e(t)$ shown in Fig.1 and let us suppose that it was plotted with 50 samples, that is to say, 50 points were necessary to represent $e(t)$ accurately.

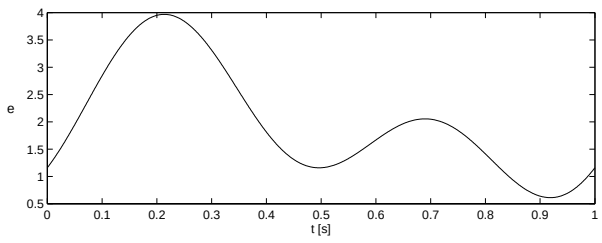

Fig.1. Envelope signal *e*(*t*)

Let us also consider the envelope modulated signal $x(t)$ shown in Fig.2, defined by

$$x(t) = e(t)\sin(2\pi f_c t),$$

with a carrier frequency $f_c = 1/T_2$ and let's suppose that 20 points were used per sinusoid. In this case the total number of samples will be $N = 20 \times f_c$. So, if

we have for example $f_c = 1\text{kHz}$, then we will obtain $N = 20\times10^3$ samples. Obviously, this number can be much larger if we increase f_c (e.g. $f_c = 1\text{MHz}$ would lead to $N = 20\times10^6$ samples).

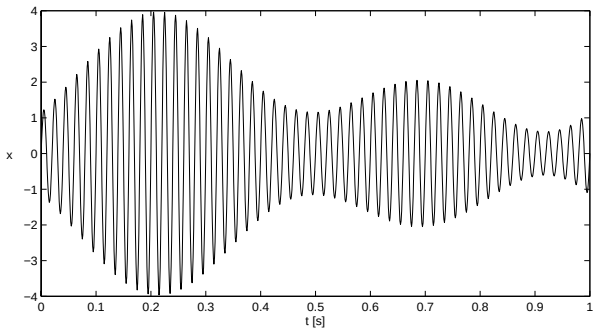

Fig.2. Envelope modulated signal $x(t)$

Consider now the bivariate representation for $x(t)$ denoted by $\hat{x}(t_1,t_2)$ and defined by

$$\hat{x}(t_1,t_2) = e(t_1)\sin(2\pi f_c t_2).$$

This function of two variables is periodic with respect to t_2, but not to t_1, i.e.

$$\hat{x}(t_1,t_2) = \hat{x}(t_1,t_2+T_2).$$

The plot of $\hat{x}(t_1,t_2)$ on the rectangle $[0,1]\times[0,T_2]$ for a carrier period $T_2 = 1\,\text{ms}$ ($f_c = 1\text{kHz}$) is shown in Fig.3 and because of its periodicity this plot repeats over the rest of the t_2 axis. We must note that $\hat{x}(t_1,t_2)$ doesn't have many undulations, unlike $x(t)$ in Fig.2. Consequently, it can be represented by relatively few samples. In fact, if we consider the same 50 sample points for $e(t)$ (t_1 dimension) and the same 20 sample points for each carrier cycle (t_2 dimension) then we will have now only $N = 50\times20 = 1000$ samples, independently of the frequency f_c. This is very significant, because considerable computation and memory savings will result from this N reduction.

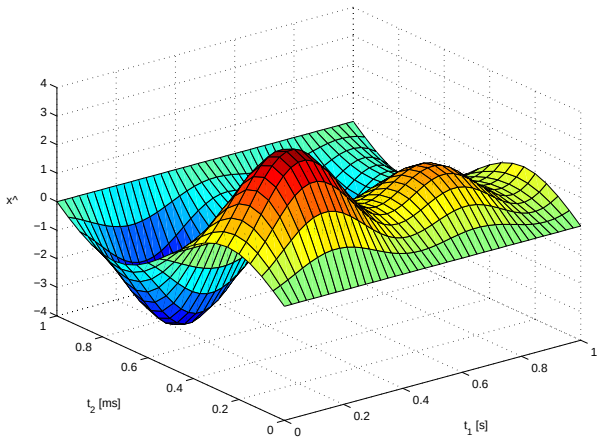

Fig.3. Bivariate representation $\hat{x}(t_1,t_2)$

Note that the original signal $x(t)$ can be easily recovered from its bivariate representation $\hat{x}(t_1,t_2)$, simply by setting $t_1 = t_2 = t$, that is to say,

$$x(t) = \hat{x}(t,t).$$

Consequently, due to the periodicity of the function $\hat{x}(t_1,t_2)$ in t_2 dimension, on the rectangular domain $[0,1]\times[0,T_2]$ we obtain

$$x(t) = \hat{x}(t, t \bmod T_2),$$

for any time value $t \in [0,1]$. Observe that as t increases from 0 to 1, the set of points given by $(t, t \bmod T_2)$ traces the sawtooth path shown in Fig.4. By noting how $\hat{x}(t_1,t_2)$ changes along this path, the behavior of $x(t)$ can be visualized.

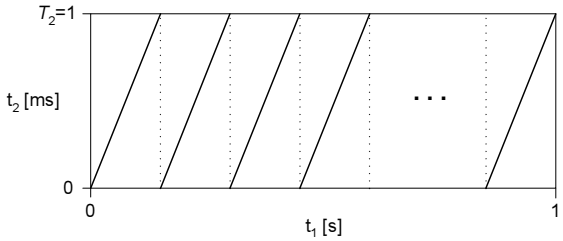

Fig.4. Path on the rectangle $[0,1]\times[0,T_2]$

2.2 Multi-Rate Partial Differential System

The discussion presented above illustrates that in spite of the sampled bivariate signal involve far fewer points than its univariate form, it contains all the information needed to recover the original signal completely. This way the ordinary differential (ODE) system (1) will be converted to the multi-rate partial differential (MPDE) system

$$p(\hat{y}(t_1,t_2)) + \frac{\partial q(\hat{y}(t_1,t_2))}{\partial t_1} + \frac{\partial q(\hat{y}(t_1,t_2))}{\partial t_2} = \\ = \hat{x}(t_1,t_2). \quad (2)$$

Then, if we want the original univariate solution $y(t)$ for a generic interval $0 \le t \le t_s$, we must solve (2) on the rectangular region $[0,t_s]\times[0,T_2]$ of t_1,t_2 space, with the following initial and boundary conditions:

$$\hat{y}(0,t_2) = g(t_2), \quad (3)$$

$$\hat{y}(t_1,0) = \hat{y}(t_1,T_2). \quad (4)$$

$g(\cdot)$ is any given initial-condition function and (4) appears due to the periodicity of the problem in t_2 dimension. The univariate solution $y(t)$ may then be recovered from its bivariate form $\hat{y}(t_1,t_2)$, simply by setting $y(t) = \hat{y}(t, t \bmod T_2)$.

The mathematical relation between the ODE system (1) and the MPDE system (2) is established by the following theorems:

Theorem 1 *If* $\hat{y}(t_1,t_2)$ *and* $\hat{x}(t_1,t_2)$ *satisfy the MPDE system (2), then* $y(t)=\hat{y}(t+c_1,t+c_2)$ *and* $x(t)=\hat{x}(t+c_1,t+c_2)$ *satisfy the ODE system (1), for any fixed* $c_1,c_2\in\mathbb{R}$.

Proof: Since $q(y(t))=q(\hat{y}(t+c_1,t+c_2))$, then we have

$$\frac{dq(y(t))}{dt}=\left.\frac{\partial q(\hat{y}(t_1,t_2))}{\partial t_1}\right|_{(t_1,t_2)=(t+c_1,t+c_2)}\cdot\frac{dt_1}{dt}+\left.\frac{\partial q(\hat{y}(t_1,t_2))}{\partial t_2}\right|_{(t_1,t_2)=(t+c_1,t+c_2)}\cdot\frac{dt_2}{dt}.$$

Now, once $\frac{dt_1}{dt}=\frac{dt_2}{dt}=1$, according to (2) we obtain

$$\frac{dq(y(t))}{dt}=\hat{x}(t_1,t_2)\big|_{(t_1,t_2)=(t+c_1,t+c_2)}-p(\hat{y}(t_1,t_2))\big|_{(t_1,t_2)=(t+c_1,t+c_2)},$$

that is to say,

$$\frac{dq(y(t))}{dt}=\hat{x}(t+c_1,t+c_2)-p(\hat{y}(t+c_1,t+c_2))=x(t)-p(y(t))$$

and consequently

$$p(y(t))+\frac{dq(y(t))}{dt}=x(t).\qquad\square$$

Theorem 2 *If the ODE system (1) has a unique solution* $y(t)$ *for an excitation* $x(t)$ *given any initial condition, then the solution* $\hat{y}(t_1,t_2)$ *of the MPDE system (2) is also unique (if it exists), given the initial and periodic boundary conditions (3) and (4).*

Proof: Theorem 1 tells us that the one-dimensional solutions $y(t)$ are given by $y(t)=\hat{y}(t+c_1,t+c_2)$, meaning that they are obtained along diagonal lines $(t+c_1,t+c_2)$ in the t_1,t_2 space, where $\hat{y}(t_1,t_2)$ are the MPDE solutions with an initial condition $y(0)$ given by $y(0)=\hat{y}(c_1,c_2)=g(c_2)$. Thus, on the diagonal lines passing through each point (c_1,c_2) in the initial condition region $c_1\times[0,T_2]$, the MPDE has a unique solution, since the ODE has a unique solution. Now, in view of the fact that $\hat{y}(t_1,t_2)$ is periodic with respect to t_2, its value at any point (t_1,t_2) is equal to that at some point along one of the diagonal lines above (this leads to a sawtooth path on the rectangular region $[0,t_s]\times[0,T_2]$). Consequently the solution $\hat{y}(t_1,t_2)$ is unique. $\square$

3 Numerical Solution of the MPDE

We will now present some efficient methods for solving (2)-(4), based on the bivariate strategy introduced in the previous section. The first three ones operate purely in the time domain. The last one is used to solve the MPDE for t_1 dimension in the time domain and for t_2 dimension in the frequency domain.

3.1 Finite Differences Method

Let us consider the set of grid points (t_{1_i},t_{2_j}) defined on the rectangle $[0,t_s]\times[0,T_2]$ by

$$0=t_{1_0}<t_{1_1}<\cdots<t_{1_i}<\cdots<t_{1_{K_S}}=t_s,\qquad(5)$$

$$0=t_{2_0}<t_{2_1}<\cdots<t_{2_j}<\cdots<t_{2_{K_2}}=T_2,\qquad(6)$$

with

$$h_{1_i}=t_{1_i}-t_{1_{i-1}}$$

and

$$h_{2_j}=t_{2_j}-t_{2_{j-1}}$$

the grid spacings in the t_1 and t_2 directions, respectively. By discretizing the partial differentiation operators of the MPDE collocated on the grid, we obtain a system of nonlinear algebraic equations that can be numerically solved using for example Newton-Raphson method. For instance, consider the finite difference approximation given by the backward Euler rule

$$\left.\frac{\partial q(\hat{y})}{\partial t_1}\right|_{(t_1,t_2)=(t_{1_i},t_{2_j})}\approx\frac{q(\hat{y}_{i,j})-q(\hat{y}_{i-1,j})}{h_{1_i}},$$

$$\left.\frac{\partial q(\hat{y})}{\partial t_2}\right|_{(t_1,t_2)=(t_{1_i},t_{2_j})}\approx\frac{q(\hat{y}_{i,j})-q(\hat{y}_{i,j-1})}{h_{2_j}},$$

with $\hat{y}_{i,j}=\hat{y}(t_{1_i},t_{2_j})$. This leads for each level i, from $i=1$ to $i=K_S$, to the scheme

$$\hat{p}_{i,j}+\frac{\hat{q}_{i,j}-\hat{q}_{i-1,j}}{h_{1_i}}+\frac{\hat{q}_{i,j}-\hat{q}_{i,j-1}}{h_{2_j}}-\hat{x}_{i,j}=0,\qquad(7)$$

$j=1,\ldots,K_2$,

where $\hat{p}_{i,j}=p(\hat{y}_{i,j})$, $\hat{q}_{i,j}=q(\hat{y}_{i,j})$ and $\hat{x}_{i,j}=\hat{x}(t_{1_i},t_{2_j})$. This way, knowing the initial solution on $i=0$ $(t_1=0)$ given by $\hat{y}_{0,j}=g(t_{2_j})$, we can find the solution on each next level i by iteratively solving (7).

We can rewrite (7) as

$$F_{i,j}=0,\quad j=1,\ldots,K_2,$$

or, equivalently,

$$F_i(Y_i)=0,$$

with

$$F_i = \begin{bmatrix} F_{i,1} & F_{i,2} & \cdots & F_{i,K_2} \end{bmatrix}^T$$

and

$$Y_i = \begin{bmatrix} Y_{i,1} & Y_{i,2} & \cdots & Y_{i,K_2} \end{bmatrix}^T.$$

If we choose for example the Newton-Raphson iterative solver, then on each iteration v we have to solve the linear system

$$J\left(Y_i^{[v]}\right)\cdot\left[Y_i^{[v+1]} - Y_i^{[v]}\right] = -F_i\left(Y_i^{[v]}\right)$$

where

$$J = \frac{dF_i}{dY_i}$$

is the Jacobian matrix of $F_i(\cdot)$.

In the scalar case the Jacobian is a $K_2 \times K_2$ sparse matrix and according to (7) it's not difficult to verify that it is given by

$$J = \begin{bmatrix} D_1 & & & L_1 \\ L_2 & D_2 & & \\ & \ddots & \ddots & \\ & & L_{K_2} & D_{K_2} \end{bmatrix}$$

where

$$D_j = \hat{p}'_{i,j} + \frac{\hat{q}'_{i,j}}{h_{1_i}} + \frac{\hat{q}'_{i,j}}{h_{2_j}}$$

and

$$L_j = -\frac{\hat{q}'_{i,j-1}}{h_{2_j}},$$

with $\hat{p}'_{i,j} = p'\left(\hat{y}_{i,j}\right)$ and $\hat{q}'_{i,j} = q'\left(\hat{y}_{i,j}\right)$.

3.2 Method of Lines

Consider the semi-discretization of $[0,t_s]\times[0,T_2]$ defined by (6). Thus, by discretizing the MPDE (2) only in t_2, we obtain an ordinary differential system in t_1 dimension, that can be time-step integrated with an initial value solver (e.g. Runge-Kutta [1]). If we use, once again, finite difference approximations based on the backward Euler rule then we have

$$p\left(\hat{y}_j(t_1)\right) + \frac{dq\left(\hat{y}_j(t_1)\right)}{dt_1} + \frac{q\left(\hat{y}_j(t_1)\right) - q\left(\hat{y}_{j-1}(t_1)\right)}{h_{2_j}} = \\ = \hat{x}_j(t_1), \quad j = 1,\ldots,K_2, \qquad (8)$$

where $\hat{y}_j(t_1) = \hat{y}\left(t_1, t_{2_j}\right)$ and $\hat{x}_j(t_1) = \hat{x}\left(t_1, t_{2_j}\right)$. Now, according to the chain rule

$$\frac{dq\left(\hat{y}_j(t_1)\right)}{dt_1} = \left.\frac{dq}{dy}\right|_{y=\hat{y}_j(t_1)} \hat{y}'_j(t_1),$$

(8) can be described in the classical form

$$\hat{y}' = f(t_1, \hat{y}), \quad 0 \le t_1 \le t_s,$$
$$\hat{y}(0) = \hat{y}_{0,}$$

which in this case results in

$$\hat{y}'_1(t_1) = \left[\hat{x}_1(t_1) - p\left(\hat{y}_1(t_1)\right) - \frac{q\left(\hat{y}_1(t_1)\right) - q\left(\hat{y}_{K_2}(t_1)\right)}{h_{2_1}}\right] \left[\left.\frac{dq}{dy}\right|_{y=\hat{y}_1(t_1)}\right]^{-1}$$

$$\hat{y}'_2(t_1) = \left[\hat{x}_2(t_1) - p\left(\hat{y}_2(t_1)\right) - \frac{q\left(\hat{y}_2(t_1)\right) - q\left(\hat{y}_1(t_1)\right)}{h_{2_2}}\right] \left[\left.\frac{dq}{dy}\right|_{y=\hat{y}_2(t_1)}\right]^{-1}$$

$$\vdots$$

$$\hat{y}'_{K_2}(t_1) = \left[\hat{x}_{K_2}(t_1) - p\left(\hat{y}_{K_2}(t_1)\right) - \frac{q\left(\hat{y}_{K_2}(t_1)\right) - q\left(\hat{y}_{K_2-1}(t_1)\right)}{h_{2_{K_2}}}\right] \left[\left.\frac{dq}{dy}\right|_{y=\hat{y}_{K_2}(t_1)}\right]^{-1}$$

with $\hat{y}_0 = \left[g\left(t_{2_1}\right), \ldots, g\left(t_{2_{K_2}}\right)\right]^T$.

3.3 Shooting

Consider now the semi-discretization of the rectangle $[0,t_s]\times[0,T_2]$ defined by (5). By discretizing the MPDE (2) only in t_1 dimension, we obtain for each level t_{1_i} an ordinary differential system in t_2, with periodic boundary conditions. If we use again the backward Euler rule then we have for each i, from $i=1$ to $i=K_S$, the boundary value problem

$$p\left(\hat{y}_i(t_2)\right) + \frac{q\left(\hat{y}_i(t_2)\right) - q\left(\hat{y}_{i-1}(t_2)\right)}{h_{1_i}} + \frac{dq\left(\hat{y}_i(t_2)\right)}{dt_2} = \\ = \hat{x}_i(t_2), \qquad (9)$$

$$\hat{y}_i(0) = \hat{y}_i(T_2), \qquad (10)$$

where $\hat{y}_i(t_2) = \hat{y}\left(t_{1_i}, t_2\right)$ and $\hat{x}_i(t_2) = \hat{x}\left(t_{1_i}, t_2\right)$. This means that once $\hat{y}_{i-1}(t_2)$ is known, the solution on next level, $\hat{y}_i(t_2)$, is achieved by solving (9)-(10). However, we must note that if we use an initial value solver (Runge-Kutta or another time-step integrator) with step size control (automatically adjusting its step lengths in order to achieve a prescribed tolerance for the error), then we will have an irregular grid with different grid point values t_{2_j} (unequal discretizing of the t_2 time axis) on successive levels t_{1_i}. This means that when solving (9)-(10) we have to interpolate the numerical solution $\hat{y}_{i-1}(t_2)$ for obtaining the

numerical solution $\hat{y}_i(t_2)$. Nevertheless, obviously for obtaining the whole solution $\hat{y}$ in the entire domain $[0,t_s]\times[0,T_2]$ we have to solve a totality of K_S boundary value problems. Here we propose to solve (9)-(10) using classical shooting [2], [5].

Shooting is an iterative solver that uses an initial value technique to solve a boundary value problem. In our case we have periodic boundary conditions and the problem can be formulated in the following way: what initial condition, or left boundary $\hat{y}_i(0)$, should be selected for time-step integration, that would lead to a final condition, or right boundary, satisfying $\hat{y}_i(T_2)=\hat{y}_i(0)$? Shooting is, in fact, a procedure that consists in guessing the initial estimate, by comparing and wisely updating the initial condition after successive time-step integrations. One possible way to do so consists in starting from a predetermined $\hat{y}_i^{[0]}(0)$ and successively making

$$\hat{y}_i^{[1]}(0)=\hat{y}_i^{[0]}(T_2),\quad \hat{y}_i^{[2]}(0)=\hat{y}_i^{[1]}(T_2),\quad \ldots$$

that is to say,

$$\hat{y}_i^{[v+1]}(0)=\hat{y}_i^{[v]}(T_2),$$

until

$$\left\|\hat{y}_i^{[f]}(T_2)-\hat{y}_i^{[f]}(0)\right\|<Tol,$$

with Tol a permitted tolerance for the error. If we define $\phi:\mathbb{R}^n\to\mathbb{R}^n$, such that

$$\hat{y}_i(T_2)=\phi\left(\hat{y}_i(0)\right),$$

then this natural initial condition update algorithm can be understood as the iterative solving of

$$\phi\left(\hat{y}_i(0)\right)=\hat{y}_i(0) \tag{11}$$

using the fixed point iteration method.

Another way to guess the initial condition $\hat{y}_i(0)$ consists in making use of the Newton-Raphson iterative solver to get the solution of (11). In such case, rewriting (11) as

$$F\left(\hat{y}_i(0)\right)=\phi\left(\hat{y}_i(0)\right)-\hat{y}_i(0)=0$$

Newton iterations take the form

$$\hat{y}_i^{[v+1]}(0)=\hat{y}_i^{[v]}(0)-J^{-1}\left(\hat{y}_i^{[v]}(0)\right)\cdot F\left(\hat{y}_i^{[v]}(0)\right),$$

where the Jacobian matrix is given by

$$J\left(\hat{y}_i^{[v]}(0)\right)=\frac{dF}{d\hat{y}_i(0)}\left(\hat{y}_i^{[v]}(0)\right)=\frac{d\phi}{d\hat{y}_i(0)}\left(\hat{y}_i^{[v]}(0)\right)-I$$

with I the $n\times n$ identity matrix. In practice, it is more efficient not to invert J but instead use for example LU decomposition to solve, at each step of the iteration, the linear algebraic system

$$J\left(\hat{y}_i^{[v]}(0)\right)\cdot\left[\hat{y}_i^{[v+1]}(0)-\hat{y}_i^{[v]}(0)\right]=-F\left(\hat{y}_i^{[v]}(0)\right).$$

Newton iteration is considerably more expensive on computing time than is fixed point iteration. Each step of the later costs just one function evaluation, whereas each step of the former calls for the updating of the Jacobian and a new LU decomposition and back substitution. However, if the function ϕ is linear or quasi-linear, the Newton-Raphson iterative solver becomes more efficient than the fixed point iteration method.

3.4 Mixed Frequency-Time Method

Let us return again to (9)-(10). We will now propose to solve each one of these boundary value problems using harmonic balance (HB) [2], [5]. HB is a classical solver commonly used in RF and microwave circuit simulation, which uses a linear combination of sinusoids to build the solution, by expanding all waveforms in Fourier series.

For simplicity let us suppose, instead of (9)-(10), a general univariate boundary value problem with periodic boundary conditions, defined by

$$p\left(y(t)\right)+\frac{dq\left(y(t)\right)}{dt}=x(t), \tag{12}$$

$$y(0)=y(T_0). \tag{13}$$

If the excitation $x(t)$ and the solution $y(t)$ are both periodic of fundamental frequency $\omega_0=2\pi/T_0$, they can be expressed by their Fourier series

$$x(t)=\sum_{k=-\infty}^{+\infty}X_k e^{jk\omega_0 t},\quad y(t)=\sum_{k=-\infty}^{+\infty}Y_k e^{jk\omega_0 t}. \tag{14}$$

Truncating the harmonics at $K\omega_0$ and substituting (14) in (12) we obtain

$$p\left(\sum_{k=-K}^{+K}Y_k e^{jk\omega_0 t}\right)+\frac{d}{dt}\left[q\left(\sum_{k=-K}^{+K}Y_k e^{jk\omega_0 t}\right)\right]=\sum_{k=-K}^{+K}X_k e^{jk\omega_0 t}.$$

As it can be seen in detail for example in [5], the HB method consists in transforming this equation entirely to the frequency domain, in order to obtain

$$\mathbf{F}(\mathbf{Y})=\mathbf{P}(\mathbf{Y})+j\boldsymbol{\Omega}\mathbf{Q}(\mathbf{Y})-\mathbf{X}=0, \tag{15}$$

where $\mathbf{X}$ and $\mathbf{Y}$ stand for the vectors with the Fourier coefficients of the excitation and the solution

$$\mathbf{X}=\begin{bmatrix}X_{-K} & \cdots & X_0 & \cdots & X_K\end{bmatrix}^T$$

$$\mathbf{Y}=\begin{bmatrix}Y_{-K} & \cdots & Y_0 & \cdots & Y_K\end{bmatrix}^T$$

and

$$j\boldsymbol{\Omega}=\begin{bmatrix}-jK\omega_0 & \cdots & 0\\ \vdots & j0 & \vdots\\ 0 & \cdots & jK\omega_0\end{bmatrix}.$$

The solution of the harmonic balance equation (15) is usually achieved by two similar iterative strategies, known as source stepping and harmonic-Newton algorithms. The first one tries to find the solution by successively solving partial linear problems obtained by increasing the magnitude of a reduced version of the excitation. The second one attempts to solve (15) by Newton-Raphson iteration for the full excitation, leading to

$$\mathbf{Y}^{[\nu+1]} = \mathbf{Y}^{[\nu]} - \left[\mathbf{J}\left(\mathbf{Y}^{[\nu]}\right)\right]^{-1} \cdot \mathbf{F}\left(\mathbf{Y}^{[\nu]}\right),$$

until

$$\left\|\mathbf{F}\left(\mathbf{Y}^{[f]}\right)\right\| < Tol,$$

where

$$\mathbf{J}\left(\mathbf{Y}^{[\nu]}\right) = \left.\frac{d\mathbf{F}}{d\mathbf{Y}}\right|_{\mathbf{Y}=\mathbf{Y}^{[\nu]}} = \mathbf{G}^{[\nu]} + j\boldsymbol{\Omega}\mathbf{C}^{[\nu]}$$

with $\mathbf{G}$ and $\mathbf{C}$ the Toeplitz [5] matrices of dp/dy and dq/dy, respectively.

Now let us return to the problem (9)-(10). In this case, for each time-step t_{1_i} we will have an HB equation

$$\mathbf{P}\left(\hat{\mathbf{Y}}_i\right) + \frac{\mathbf{Q}\left(\hat{\mathbf{Y}}_i\right) - \mathbf{Q}\left(\hat{\mathbf{Y}}_{i-1}\right)}{h_{1_i}} + j\boldsymbol{\Omega}\mathbf{Q}\left(\hat{\mathbf{Y}}_i\right) = \hat{\mathbf{X}}_i,$$

where $\hat{\mathbf{X}}_i$ and $\hat{\mathbf{Y}}_i$ are the vectors with the Fourier coefficients for the excitation and the solution on level i. So, we have a mixed mode technique that handles the envelope (t_1 dimension) in the time domain and the carrier (t_2 dimension) in the frequency domain.

4 Experimental Results

4.1 Sample Application

In order to test the efficiency of the methods presented in the previous section, we propose the nonlinear single node circuit of Fig.5.

Beyond the power source i_S, this circuit is composed by a linear conductance, a nonlinear capacitance and a nonlinear current source. The characteristics of the nonlinear elements are modeled in the following way:

- For the current we considered a nonlinear voltage-dependent current source

$$i_{NL}\left(v_O(t)\right) = I_0 \tanh\left(\alpha v_O(t)\right). \qquad (16)$$

- For the capacitance we considered that

$$q_{NL}\left(v_O(t)\right) = \tau_F i_{NL}\left(v_O(t)\right), \qquad (17)$$

which means that the storage charge is proportional to the conductive current. Thus,

$$C\left(v_O(t)\right) = \frac{dq_{NL}\left(v_O(t)\right)}{dv_O(t)} = \tau_F I_0 \alpha \operatorname{sech}^2\left(\alpha v_O(t)\right).$$

These nonlinear models are usually encountered in doped semiconductors (e.g. saturating velocity field resistors and junction diffusion capacitances). The forms of $i_{NL}\left(v_O(t)\right)$ and $C\left(v_O(t)\right)$ are plotted in Fig.6 and Fig.7, respectively.

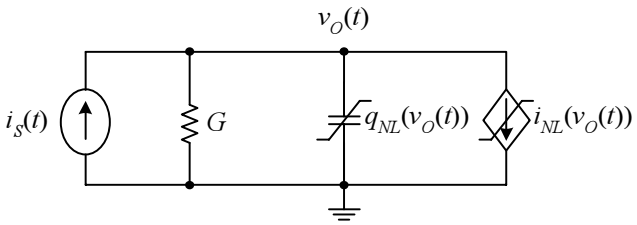

Fig.5. Nonlinear circuit example

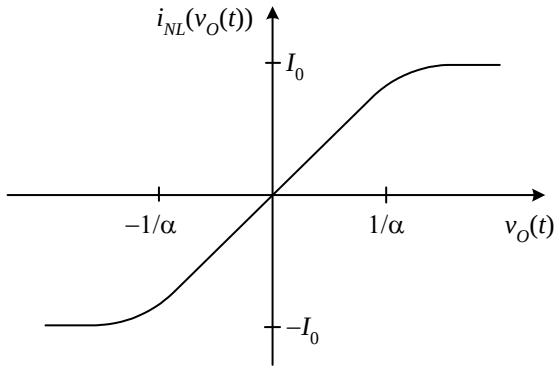

Fig.6. Nonlinear current

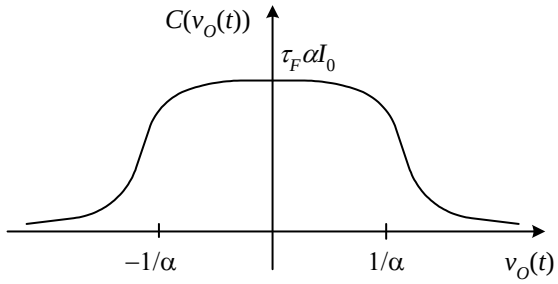

Fig.7. Nonlinear capacitance

4.2 Mathematical Model

The mathematical model of an electronic circuit is based on Kirchhoff's current and voltage laws:

- Kirchhoff's current law: "The net current into any node is zero".
- Kirchhoff's voltage law: "The net sum of the voltage drops around any closed loop is zero".

In this case we have a simple single node circuit and we only need to apply the Kirchhoff's current law to the node v_O. Doing so, we can say that the nodal analysis of the circuit leads to

$$i_G + i_C + i_{NL} = i_S . \qquad (18)$$

The conductance G is assumed as linear and is thus characterized by a proportional relation between its terminal voltage and current, that is to say,

$$i_G(t) = G v_O(t), \qquad (19)$$

known as Ohm's law. For the nonlinear capacitance we have

$$i_C(t) = \frac{dq_{NL}(v_O(t))}{dt} \qquad (20)$$

for the fundamental relation between its current and charge. Substituting (19) and (20) in (18) we obtain the following ordinary differential equation:

$$G v_O(t) + \frac{dq_{NL}(v_O(t))}{dt} + i_{NL}(v_O(t)) = i_S(t).$$

Finally, since the nonlinear charge $q_{NL}(v_O(t))$ and current $i_{NL}(v_O(t))$ are modeled by (17) and (16), we can write

$$G v_O(t) + \alpha \tau_F I_0 \operatorname{sech}^2(\alpha v_O(t)) \frac{dv_O(t)}{dt} + I_0 \tanh(\alpha v_O(t)) = i_S(t). \qquad (21)$$

4.3 Numerical Simulation Results

The circuit of Fig.5 was simulated in *MATLAB*® from $t = 0$ to $t = 1000$ ms, for $G = 1\,\text{m}\Omega^{-1}$, $I_0 = 0.4$ mA, $\alpha = 1\,\text{V}^{-1}$, $\tau_F = 2 \cdot 10^{-3}$ s and an excitation

$$i_S(t) = e(t)\sin(2\pi f_c t) \text{ mA},$$

with a carrier frequency $f_c = 1$ kHz and an envelope $e(t) = 5\sin(2\pi f t)$, $f = 0.5$ Hz.

The values of G, I_0, α and τ_F were chosen in way to obtain a considerably nonlinear problem and the overall results of this simulation are presented in Table 1 where, for comparison, we also included a non multi-rate method (classical univariate time-step integration). As we can see, the multi-rate methods presented in Section 3 exhibit significant advantages in speed over the non multi-rate method. In fact, while in the MPDE based methods we have total computation times ranging from 0.18 to 2.49 seconds, in the univariate time-step integration we have 15.93 seconds.

In order to test the accuracy of the methods a reference solution was achieved by numerically solving the ODE (21) via classical univariate time-step integration, using an embedded Runge-Kutta [1] method of higher order, with an extremely small time step.

Method	time[1] (sec)	error $\|\cdot\|_\infty$	error $\|\cdot\|_{L^2}$
Finite differences	1.82	0.0583	0.0407
Method of lines	2.49	0.0664	0.0491
Shooting	2.32	0.0378	0.0129
Mixed (freq. - time)	0.18	0.0256	0.0072
Univariate	15.93	0.0328	0.0199

Table 1. Numerical simulation results

The bivariate solution is shown in Fig.8 and the univariate solution is of the type of the one plotted in Fig.9.

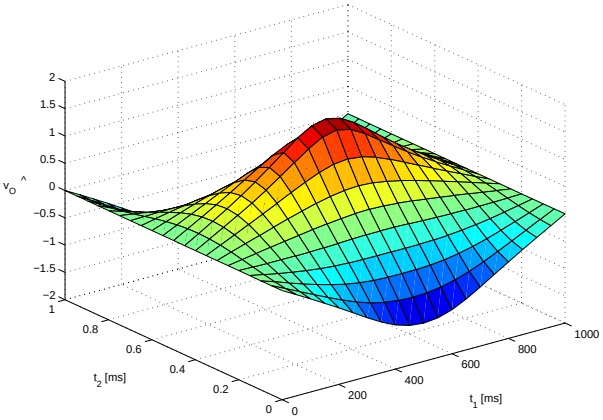

Fig.8. Bivariate solution, $\hat{v}_O(t_1, t_2)$

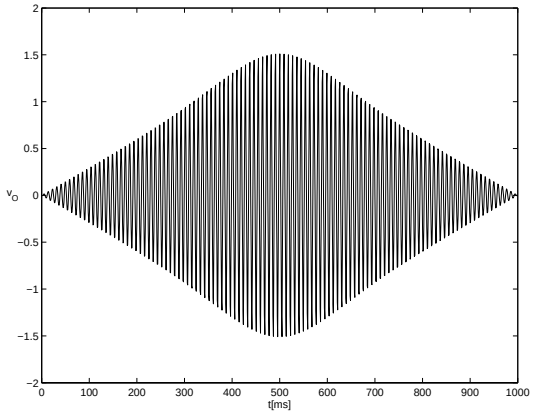

Fig.9. Univariate solution $v_O(t)$

In order to have a more realistic and accurate idea of the solution, a time scaled version of $v_O(t)$ in the interval [498,500]ms is plotted in Fig.10. The reason why we chose this particular interval is because the nonlinearity effects are stronger here (maximum excitation).

[1] Computation time (AMD Athlon 1.8 GHz, 256MB RAM).

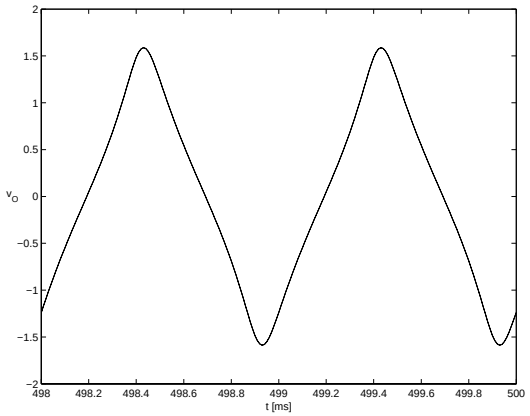

Fig.10. Univariate solution $v_O(t)$, in [498,500]ms

We have tested other values of G, I_0, α and τ_F, leading to weakly nonlinear and quasi-linear problems, and the results were similar to the ones presented in Table 1: multi-rate methods were always much faster than the univariate one and an excellent speedup was exhibited by the mixed (frequency-time) method. However, the extreme efficiency of this mixed method cannot be generalized. In fact, if for a fixed excitation we successively increase the value of α or decrease the values of G and I_0, the circuit nonlinearities become stronger and the method looses efficiency. We have simulated the problem with $G = 0.74\,\mathrm{m\Omega^{-1}}$, $I_0 = 0.155\,\mathrm{mA}$, $\alpha = 2\,\mathrm{V^{-1}}$ and $\tau_F = 5\cdot 10^{-3}\,\mathrm{s}$, and we obtained a total of 4.98 seconds for the computation time of the mixed method, while for example in the finite differences method this time was 1.99 seconds. Furthermore, if we try to decrease the values of G or I_0 the solution cannot even be found by the mixed method.

5 Conclusions

Multi-rate methods have demonstrated to be much more efficient than the classical univariate method. It is so because they are based in a powerful strategy that uses two time variables to describe multi-rate behavior. Efficiency is achieved without compromising accuracy and considerable speedups are obtained. The mixed (frequency-time) method is extremely efficient for solving weakly nonlinear or quasi-linear circuits, but may become inefficient for solving strongly nonlinear circuits. In fact, under strong nonlinearities frequency methods become even useless because they require a large number of harmonics in Fourier expansions. Sharp features like spikes or pulses generated by highly nonlinear circuits are not represented efficiently in a Fourier basis.

References:

[1] E. Hairer, S. Nørsett and G. Wanner, *Solving Ordinary Differential Equations I: Nonstiff Problems*, Springer-Verlag, Berlin, 1987.

[2] K. Kundert, J. White and A. Sangiovanni-Vincentelli, *Steady-State Methods for Simulating Analog and Microwave Circuits*, Kluwer Academic Publishers, Norwell, 1990.

[3] J. Oliveira, *Métodos Multi-Ritmo na Análise e Simulação de Circuitos Electrónicos não Lineares*, Master Thesis, Department of Mathematics, University of Coimbra, 2004.

[4] J. C. Pedro and N. B. Carvalho, A mixed-mode simulation technique for the analysis of RF circuits driven by modulated signals, *III Conferência de Telecomunicações*, Figueira da Foz, 2001.

[5] J. C. Pedro and N. B. Carvalho, *Intermodulation Distortion in Microwave and Wireless Circuits*, Artech House Inc., Norwood, 2003.

[6] J. Roychowdhury, Efficient methods for simulating highly nonlinear multirate circuits, *34th Design Automation Conference*, Anaheim, 1997.

[7] J. Roychowdhury, Analyzing circuits with widely separated time scales using numerical PDE methods, *IEEE Transactions on Circuits and Systems*, Vol.5, No.48, 2001, pp. 578-594.

[8] G. D. Smith, *Numerical Solution of Partial Differential Equations: Finite Difference Methods*, Oxford University Press, Oxford, 1993.